Modeling and understanding of the thermal failure induced by high power microwave in CMOS inverter*

Yu-Hang Zhang(张宇航)†, Chang-Chun Chai(柴常春), Yang Liu(刘阳), Yin-Tang Yang(杨银堂), Chun-Lei Shi(史春蕾), Qing-Yang Fan(樊庆扬), and Yu-Qian Liu(刘彧千)

Key Laboratory of Ministry of Education for Wide Band-Gap Semiconductor Materials and Devices, School of Microelectronics, Xidian University, Xi'an 710071, *China*

(Received 3 December 2016; revised manuscript received 18 January 2017; published online 6 April 2017)

The thermal failure induced by high power microwave (HPM) in a complementary metal oxide semiconductor (CMOS) inverter is investigated and its dependence on microwave parameters is discussed in detail. An analytical model of the temperature distribution is established and the relationships between hotspot temperature and pulse width and between hotspot temperature and frequency are predicted, which reveals a more severe rise in temperature under the influence of microwave with longer width and lower frequency. The temperature variation mechanism and the theoretical temperature model are validated and explained by the simulation. Furthermore, variation trend of damage threshold with microwave parameters is derived theoretically, and the conclusions are consistent with simulation results and reported data.

Keywords: temperature model, microwave damage, pulse width, frequency effect

PACS: 85.30.Tv, 84.40.–x **DOI:** 10.1088/1674-1056/26/5/058502

1. Introduction

As the integrated circuit is used more and more widely in civil and military fields, research on microelectronic reliability has been a hotspot in recent years. The failures caused on the semiconductor could be various, such as a material defect, device aging and radical external excitation. High power microwave is a typical instance of electromagnetic interference with a high power level, high frequency and short width generally, and is developed rapidly for the use of microwave weapons. High power microwave (HPM) is easy to couple into electronic system via antennas, cables and apertures of shells intentionally or unintentionally, leading to degeneration in performance and temporary or permanent failure.[1]

Since the external microwave may induce a catastrophic impact, the microwave effects on various integrated circuits and semiconductors have widely been investigated in these last few years. Many experimental researches were carried out through testing the damage susceptibility of discrete PIN diode,[2] high electron mobility transistor (HEMT),[3,4] bipolar transistor,[5] integrated components on transistor–transistor logic (TTL) and CMOS logic,[6] computer system,[7] etc. Besides, theoretical studies were also presented widely. Ren *et al.* reported the motion of current filaments and the thermal failure effect of PIN diode under electromagnetic pulse.[8] Liu *et al.*[9,10] and Yu *et al.*[11,12] revealed the phenomena of damage and degradation as well as their mechanisms of GaAs HEMT under the influence of HPM by numerical simulation and experiment used for comparison. Chai *et al.*[13] and Ma *et al.*[14–16] proposed the thermal failure mechanism in bipolar semiconductor and proposed some measures against it. As for the CMOS device, Kim and Iliadis focused on the dynamic and static characteristics in a CMOS inverter under HPM environment.[17–20] Wang *et al.*[21] and Yu *et al.*[22–24] researched the HPM induced latch-up effect and its critical factors in experiment and theory. However, the thermal damage is also a significant failure cause for the CMOS device besides latch-up.[1]

This work focuses on the thermal failure in the CMOS inverter caused by HPM. An analytical temperature distribution is derived and the relationships between hotspot temperature and microwave frequency, and between hotspot temperature and width are predicted. Based on numerical simulation, the damage mechanism is presented and the temperature model is validated and explained. In addition, the variations of damage threshold with frequency and width are predicted and compared with simulation results and reported data.

2. Modeling procedure

A typical CMOS inverter schematic diagram with an n-well is depicted in Fig. 1. The doping types and the electrical connections are illustrated, and B, S, D, G represent bulk terminals, source terminals, drain terminals, and gate terminals of NMOS or PMOS, respectively. The top surface is regarded as being adiabatic and the lower surface is assumed to be at ambient temperature (300 K). For digital circuits, the external microwave is more likely to invade the electronic system via

*Project supported by the Open Fund of Key Laboratory of Complex Electromagnetic Environment Science and Technology, China Academy of Engineering Physics (Grant No. 2015-0214. XY.K).

†Corresponding author. E-mail: yhzhang0916@foxmail.com

© 2017 Chinese Physical Society and IOP Publishing Ltd

a back-door couple path,[1] of which power/ground lines are typical instances, thus the external HPM injection source acts on the source terminal of the NMOS part in our work. The external HPM is assumed to be a sinusoidal plane wave, which has been proved to be equivalent to actual HPM coupled with wires approximately.[25]

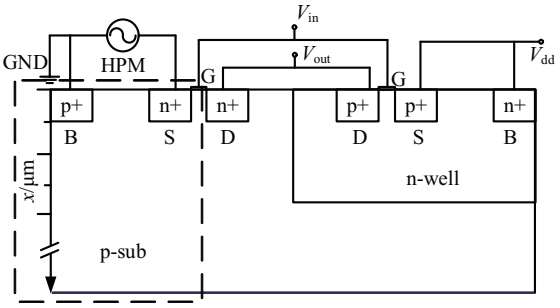


Fig. 1. Cross-section schematic of a typical CMOS inverter.

Obviously, during the positive semi-period of the external microwave, the PN junction across the bulk and source terminal becomes biased reversely, and there is only reverse current which can be ignored since an avalanche effect has not been taken into consideration. However, when the external electric potential turns negative, current paths from the bulk and source terminal near the device surface occur, leading to a Joule heat production. In this case, the temperature of this region will rise up if the heat cooling rate is less than the heat generation rate. Thus, the surface temperature presents a periodic "down-up-down" variation, and the device maybe burns out at the hotspot finally.

According to the above analysis, the rise in device temperature is due to the forward current across the "N^+–P–P^+" structure between the source and the substrate terminal during the negative semi-period of external microwave, and the hotspot is close to the top surface of the device. Therefore, it is reasonable to regard the device (NMOS side) as a one-dimensional (1D) semi-infinity vertical solid medium with the origin point located at the top surface as seen in Fig. 1 and marked by the dash line. Here, we first regard the heat induced by the forward current resulting from external HPM as a constant flux heat at x=0. Hence, the heat flux f inside the device satisfies the following equation with a Dirichlet boundary condition:[26]

$$\kappa\frac{\partial^2 f}{\partial x^2}=\frac{\partial f}{\partial t},\ \text{s.t. } f=F_0,\ \text{when } x=0,\ t>0, \tag{1}$$

where x is the vertical position, t is the time, F_0 is the equivalent boundary flux heat and κ is the thermal diffusivity which is actually relevant to temperature. For simplicity, the thermal diffusivity is assumed to be a constant in our work. The solution of Eq. (1) can be expressed as follows:[26]

$$f=F_0\mathrm{erfc}\left(\frac{x}{2\sqrt{\kappa t}}\right), \tag{2}$$

where $\mathrm{erfc}(x)$ represents the complementary error function. The temperature distribution v along the x axis, which is the integral form of heat flux, can be obtained as[26]

$$v=\frac{2F_0}{K}\left[\left(\frac{\kappa t}{\pi}\right)^{1/2}\mathrm{e}^{-x^2/4\kappa t}-\frac{x}{2}\mathrm{erfc}\frac{x}{2\sqrt{\kappa t}}\right], \tag{3}$$

where K is the thermal conductivity which is proportional to thermal diffusivity κ, and assumed to be a constant as well. However, the surface heat fluxes are periodic, which are not identical during different temperature-rise processes. During the positive semi-period of the microwave, the heat flux can be considered as zero since there is no heat production according to the previous discussion, and the border is adiabatic, whereas during the negative half of the N-th period, the heat flux is defined as F_{N-1}. Obviously, F_0 represents the equivalent heat flux during the 1st cycle of microwave now. Therefore, after N periods of microwaves, the temperature can be obtained according to the superposition principle as follows:

$$v=T_0+\sum_{i=0}^{N-1}\frac{2F_i}{K}\left[g\left(x,\left(i+\frac{1}{2}\right)T\right)-g\left(x,iT\right)\right], \tag{4}$$

where T is the period length of microwave, T_0 is the initial temperature of device (300 K), and $g(x,t)$ represents the following relationship:

$$g(x,t)=\left(\frac{\kappa t}{\pi}\right)^{1/2}\mathrm{e}^{-x^2/4\kappa t}-\frac{x}{2}\mathrm{erfc}\frac{x}{2\sqrt{\kappa t}}. \tag{5}$$

According to our previous discussion, the hotspot exists at the surface of the device, hence the max temperature is located at $x=0$, and equation (4) where $x=0$, can be expressed as follows:

$$v=T_0+\sum_{i=0}^{N-1}F_i'\left[\left(i+\frac{1}{2}\right)^{1/2}\left(\frac{1}{f}\right)^{1/2}-i^{1/2}\left(\frac{1}{f}\right)^{1/2}\right], \tag{6}$$

where F_i' is a simplified value calculated by F_i and K, f is the HPM frequency, and N is the total number of microwave periods, which is equal to f multiplied by pulse width t_{w}. The F_i' reflects the heat flux of the surface during the negative semi-period of the (i-1)th microwave period, and it is proportional to the forward current across the junction. On the other hand, the PN forward junction has a power-law relationship with temperature, that is to say, F_i' has a power law with the following expression:

$$v|_{t=(i-1)T}=T_0+\sum_{k=0}^{i-1}F_k'\left[\left(k+\frac{1}{2}\right)^{1/2}\left(\frac{1}{f}\right)^{1/2}-k^{1/2}\left(\frac{1}{f}\right)^{1/2}\right]. \tag{7}$$

Therefore, equation (6) reveals a complex relationship between v and f, and an equivalent heat flux level $\bar{F}$ is adopted in

our work, which reflects the average flux level of F_i' throughout the duration of t_w. According to Eq. (7), $\bar{F}$ can be considered as a power function of f and t_w. Hence, the max temperature inside the device under an injected microwave with a frequency f and pulse width t_w is obtained as follows:

$$v_{\max}(f,t_w) = T_0 + \bar{F}(f,t_w) \sum_{i=0}^{ft_w-1} \left[\left(i+\frac{1}{2}\right)^{1/2} \left(\frac{1}{f}\right)^{1/2} - i^{1/2} \left(\frac{1}{f}\right)^{1/2} \right]. \quad (8)$$

One thing should be noted, i.e., the injection power level is assumed to be a constant value in the above discussion, whereas it contributes to $\bar{F}$ positively actually, and the fitting coefficients are related to the injection power.

3. Simulation setup

In order to verify the validity of the above analysis, it is necessary to understand the temperature distribution inside the device in practice. Unfortunately, it is not easy to capture the temperature distribution in detail in a real semiconductor device, therefore, a simulation model is built and the phenomena are discussed physically on the basis of it in our work. The device structure is modeled (referring to Fig. 1). The gate length is specified to be 0.35 μm, and the total sizes in the horizontal and the vertical direction are 10.5 μm and 4 μm, respectively. The upper surface is adiabatic and the lower surface is kept at 300 K, which is consistent with the conditions in Section 2. The voltage transfer curve and current transfer curve are shown in Fig. 2, indicating that the inverter works at 3.3 V supply voltage with a flip threshold V_m located at 1.63 V.

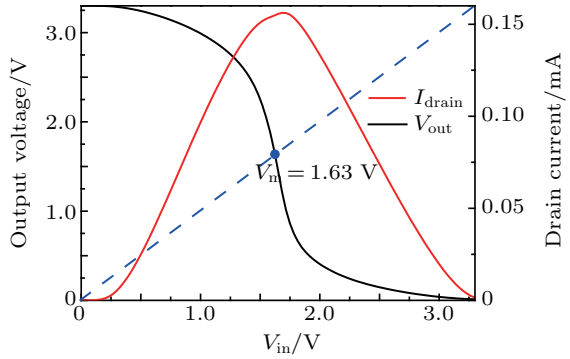


Fig. 2. (color online) Voltage transfer curve and current transfer curve of the inverter built in this work.

4. Results and discussion

4.1. Process of temperature variation

The maximum temperature inside the CMOS inverter responding to the injected microwave with a peak induced voltage of 5 V is shown in Fig. 3. The temperature curve presents a periodic "rise-fall" trend, which is consistent with the analysis in Section 2. However, the max temperature turns higher overall, and it should reach the melting point of silicon finally, leading to a partial short-circuit and invalidating the function of the device. In order to study the details of the temperature-rise process, the part of curves (from 4th ns to 5th ns) are zoomed in. The result is consistent with the analysis in Section 2, in which it can be seen that the temperature rises during the negative semi-period and it decreases during the positive semi-period. Since the variation in temperature results from Joule heat, and the rate of power depends on electric field strength and current density: these physical quantities of the NMOS side are extracted from Figs. 4 and 5.

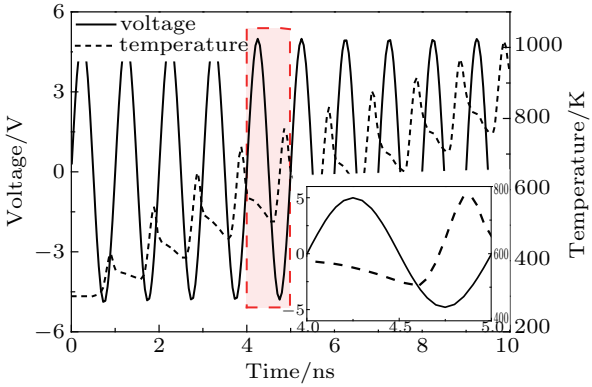


Fig. 3. (color online) Variation of max temperature with time under the action of external stimulating microwave.

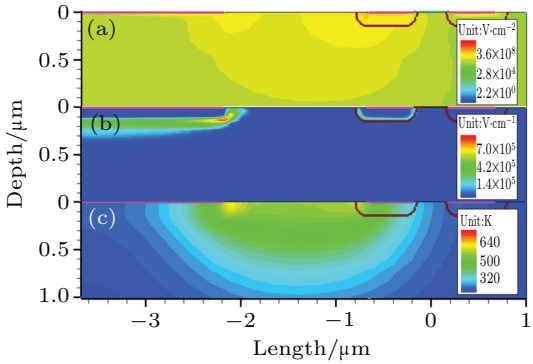


Fig. 4. (color online) Distributions of (a) current density, (b) electric field strength, and (c) temperature during positive semi-period of external microwave inside the device.

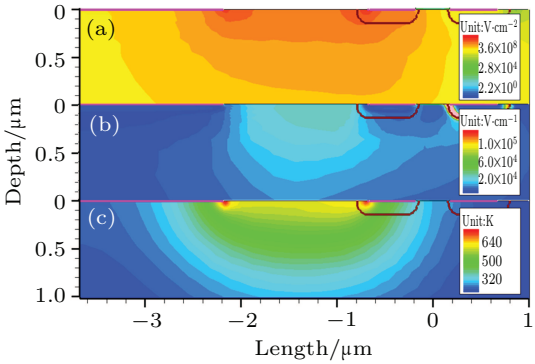


Fig. 5. (color online) Distributions of (a) current density, (b) electric field strength, and (c) temperature during negative semi-period of external microwave inside the device.

Obviously, when the external electric potential is positive, the junctions of N^+–P and P–P^+ are biased reversely, and the electric fields concentrate on depletion layers. The external voltage is divided by two junctions, and the impact ionization is not enough to trigger an avalanche effect, hence there is little current from the source to the bulk terminal. The heat flows towards the substrate, and the temperature decreases. However, when the external electric potential is negative, an apparent forward-current path forms. Since the current density is quite large, it tends to form hotspots at the junction region, where the radius of curvature of the electric field is small. Therefore, if the rate of heat generation is higher than the cooling rate, the temperature becomes higher.

4.2. Validation of the maximum temperature model

Equation (8) reveals the relationship among maximum temperature of the device and pulse width and microwave frequency. In order to verify the validity of this model, the simulated max temperatures versus microwave frequency under diverse injection power levels are shown in Fig. 6. The pulse width is specified as 10 ns, and it is seen that the max temperatures decline with frequency increasing from 0.5 GHz to 4 GHz. The analytical model (8) is used for fitting this relationship and the results are also exhibited in Fig. 6. The fitting curves show the same trends as the curve of simulated data, proving the validity of the frequency effect.

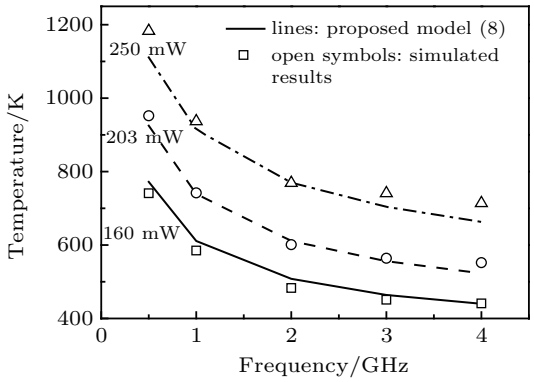


Fig. 6. Variations of max temperature with frequency under diverse microwave power levels.

Besides, the relationship between max temperature and microwave pulse width is obtained by simulation and shown in Fig. 7. The results show a positive correlation between pulse width and max temperature. It is reasonable since the temperature increases continuously under the effect of the injected microwave with a constant frequency and power level. The analytical model (8) is also presented in Fig. 7 and shows the same trend as simulated data, validating our analysis above.

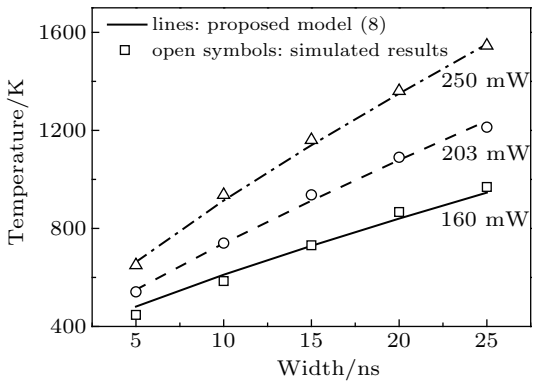


Fig. 7. Variations of max temperature with width at diverse microwave power levels.

4.3. Dependence of $\bar{F}$ on pulse width and frequency

As mentioned in Section 2, an equivalent heat flux $\bar{F}$ is adopted to represent the average heat flux in t_w duration, and it is reasonable to consider $\bar{F}$ as a power function of f and t_w. In our work, $\bar{F}$ is approximated as follows:

$$\bar{F}(f,t_w) = C_1 f^{C_2} t_w^{C_3}, \tag{9}$$

where C_2 and C_3 are calculated to be negative values and positive values, respectively, and C_1 is the value related to injected power positively. The signs of C_2 and C_3 reveal that the average heat generation rate is actually negatively related to microwave frequency and positively related to pulse width. According to the previous analysis, the heat generation behavior results from PN forward current, and the forward current is related to temperature positively. Since the peak temperature increases overall with time going by, the heat generation rate increases, that is to say, F_i' is an increasing function of i. So it is deduced that for a certain frequency and power level, $\bar{F}$ is an increasing function of microwave pulse width t_w.

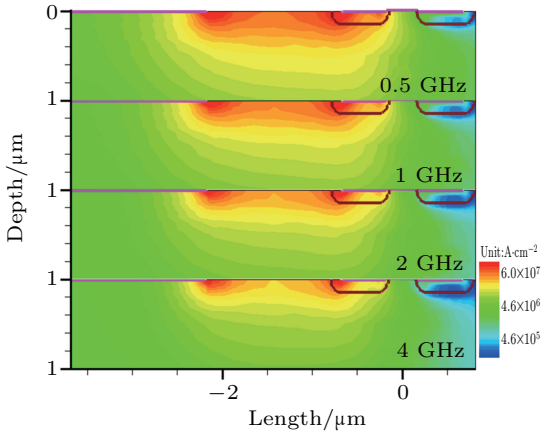


Fig. 8. (color online) Forward current densities under diverse frequency microwaves after the same period of time.

Furthermore, for a microwave with a lower frequency, the duration of each cycle is longer, and the temperature of the hotspot is larger after a temperature-rise period, leading to a larger junction current for the next cycle in turn. After the

same period of time, the temperature and the current density are both higher for lower frequency, resulting in a larger $\bar{F}$. The scenario which can be considered as positive feedback is illustrated in Fig. 8, where the current densities at microwave negative semi-period of diverse frequencies after the same period of time are shown. It is apparent that the forward current density varies with frequency reversely; therefore, $\bar{F}$ can be seen as a negative function of f, as we calculated previously.

4.4. Dependence of damage threshold on pulse width and frequency

As we mentioned in Section 2, the maximum temperature inside the device presents a periodic variation and increases overall, and it is proved that the burn-out point is located at the top surface. For a microwave with frequency and pulse width fixed, one can obtain a relationship between equivalent heat flux $\bar{F}$ and max temperature. Noticing that the forward current is apparently related to the induced voltage, $\bar{F}$ is an increasing function of induced voltage or injected power level. In Eq. (8), it is easy to prove the summation term Σ to be an increasing function of t_w, and a decreasing function of f. Hence, a larger $\bar{F}$ is needed for microwave with higher frequency and shorter pulse width to reach the silicon melt point v_m. However, f and t_w contribute to $\bar{F}$ oppositely for a certain injection power level (i.e., $\bar{F}$ actually becomes smaller with increasing f or decreasing t_w if injected power is a constant), where the trends are the same in the summation term Σ, according to the signs of C_2 and C_3 in Eq. (9). That is to say, the device damage power threshold increases with a higher frequency and a shorter pulse width. The derived conclusion is consistent with the simulation data as seen in Figs. 9 and 10. In Ref. [6] some typical CMOS integrated components were tested under diverse frequencies, and in Ref. [27] the pulse width effect of PN junction damage was investigated. The reported data are also shown in Figs. 9 and 10, which are in accordance with the conclusions in this work, and the simulated pulse width dependence satisfies the Wunsch–Bell relationship.[28] In addition, the damage energy thresholds are also calculated and given in Fig. 10, showing an increase for a longer microwave generally, and the results are consistent with those in Ref. [29]. Thus it is believed that the heat diffuses around more for a longer width, and slows down the temperature rise at hotspots.

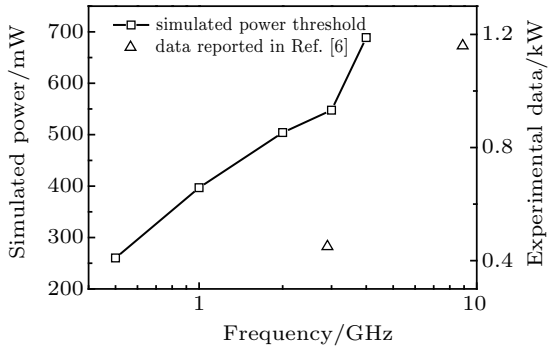


Fig. 9. Variations of simulated (empty square) and measured (empty triangle) damage power threshold with frequency.

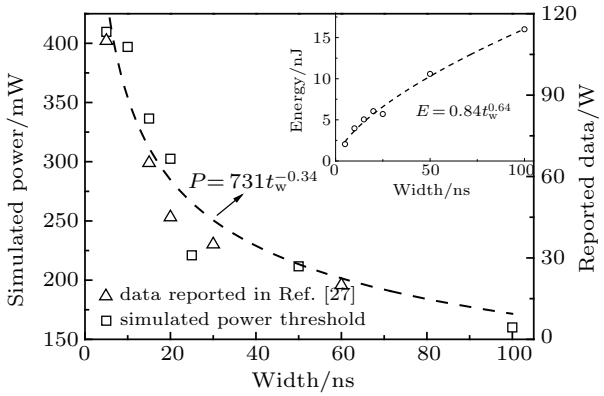


Fig. 10. Variations of simulated (empty square) damage power and energy threshold with width, and their comparisons with their counterparts of reported data (empty triangle).

5. Conclusions

A temperature rising behavior for a typical CMOS inverter under the influence of high power microwave is derived theoretically on the basis of an abstract model, and analytical hotspot temperature inside the device is presented with considering the dependence on microwave frequency and pulse width. By numerical simulation on the device model built in this work, the mechanism of temperature variation in the device is presented and the results show that forward current acts as a major heat source during the negative semi-cycle of external microwave. The simulated temperature variation trends validate the dependence on pulse width and frequency we predicted from the theoretical model, and the relationship between equivalent external heat flux and microwave parameter is explained. Furthermore, the dependence of damage threshold on frequency and width is derived based on the theoretical model, and turns out to be consistent with simulated results and reported conclusions.

References

[1] Bäckström M G and Lövvstrand K G 2004 *IEEE Trans. Electromagn. Campat.* **46** 396
[2] Zhao Z G, Ma H G, Zhao G, Wang Y and Zhong L Q 2013 *High Power Laser and Particle Beams* **25** 1741 (in Chinese)
[3] Zhang C B, Zhang J D, Wang H G and Du G X 2016 *Microelectron. Reliab.* **60** 41
[4] Li Z P, Li J, Sun J, Liu Y and Fang J Y 2016 *Acta Phys. Sin.* **65** 168501 (in Chinese)
[5] Fan J P, Zhang L and Jia X Z 2010 *High Power Laser and Particle Beams* **22** 1319 (in Chinese)
[6] Fang J Y, Shen J A, Yang Z Q and Qiao D J 2003 *High Power Laser and Particle Beams* **15** 591 (in Chinese)
[7] Nitsch D, Camp M, Sabath F, Haseborg J L and Garbe H 2004 *IEEE Trans. Electromagn. Campat.* **46** 380
[8] Ren X R, Chai C C, Ma Z Y, Yang Y T, Qiao L P, Shi C L and Ren L H 2013 *J. Semicond.* **34** 044004
[9] Liu Y, Chai C C, Yang Y T, Sun J and Li Z P 2016 *Chin. Phys. B* **25** 048504

[10] Liu Y, Chai C C, Yu X H, Fan Q Y, Yang Y T, Xi X W and Liu S B 2016 *Acta Phys. Sin.* **65** 038402 (in Chinese)
[11] Yu X H, Chai C C, Liu Y, Yang Y T and Fan Q Y 2015 *Microelectron. Reliab.* **55** 1174
[12] Yu X H, Chai C C, Liu Y, Yang Y T and Xi X W 2015 *Chin. Phys. B* **24** 048502
[13] Chai C C, Ma Z Y, Ren X R, Yang Y T, Zhao Y B and Yu X H 2013 *Chin. Phys. B* **22** 068502
[14] Ma Z Y, Chai C C, Ren X R, Yang Y T, Chen B, Song K and Zhao Y B 2012 *Chin. Phys. B* **21** 098502
[15] Ma Z Y, Chai C C, Ren X R, Yang Y T, Chen B and Zhao Y B 2012 *Chin. Phys. B* **21** 058502
[16] Ma Z Y, Chai C C, Ren X R, Yang Y T, Zhao Y B and Qiao L P 2013 *Chin. Phys. B* **22** 028502
[17] Kim K and Iliadis A A 2007 *IEEE Trans. Electromagn. Campat.* **49** 876
[18] Kim K and Iliadis A A 2008 *Solid State Electron.* **52** 1589
[19] Kim K and Iliadis A A 2010 *Solid State Electron.* **54** 18
[20] Iliadis A A and Kim K 2010 *IEEE Trans. Dev. Mater. Reliab.* **10** 347
[21] Wang H, Li J, Li H, Xiao K and Chen H 2008 *PIER* **87** 313
[22] Yu X H, Chai C C, Ren X R, Yang Y T, Xi X W and Liu Y 2014 *J. Semicond.* **35** 084011
[23] Yu X H, Chai C C, Liu Y and Yang Y T 2015 *China Inform Sci.* **58** 082402
[24] Yu X H, Chai C C, Qiao L P, Yang Y T, Liu Y and Xi X W 2015 *J. Semicond.* **36** 054011
[25] Korte S, Camp M and Garbe H 2005 *IEEE International Symposium on Electromagnetic Compatibility*, August 8–12 2005, Chicago, IL, p. 489
[26] Carslaw H S and Jaeger J C 1959 *Conduction of Heat in Solids*, 2nd edn. (Oxford: Clarendon press) p. 75
[27] Li P, Liu G Z, Huang W H and Wang L P 2001 *High Power Laser and Particle Beams* **13** 353 (in Chinese)
[28] Wunsch D C and Bell R R 1968 *IEEE Trans. Nucl. Sci.* **15** 244
[29] Yu X H 2015 *Research on the HPM Effects of CMOS Inverter and GaAs HEMT Device* (Ph.D. Dissertation) (Xi'an: Xidian University) (in Chinese)